Acta Pharmaceutica Sinica B 2026;16(2):900−912

Chinese Pharmaceutical Association
Institute of Materia Medica, Chinese Academy of Medical Sciences

Acta Pharmaceutica Sinica B

www.elsevier.com/locate/apsb
www.sciencedirect.com

ORIGINAL ARTICLE

A novel fusion protein of COVID-19 virus enhancing protection of Syrian hamsters infected with SARS-CoV-2

Hanlu Wang[a,b], Tiantian Yang[a], Yichao Yan[b], Fengmei Yang[c], Xunhuan Song[d], Shuning Zhang[b], Wenhong Jiang[b], Mingxue Li[c], Wenting Sun[c], Yanyan Li[c], Weihua Jin[c], Suqin Duan[c], Meng Qin[a,d,*], Zhanlong He[c,*], Yongping Jiang[a,b,*]

[a]*Biopharmaceutical R&D Center, Chinese Academy of Medical Sciences, Peking Union Medical College, Suzhou 215126, China*
[b]*Biopharmagen Corp., Suzhou 215126, China*
[c]*Institute of Medical Biology, Chinese Academy of Medical Sciences, Peking Union Medical College, Yunnan Key Laboratory of Vaccine Research Development on Severe Infectious Disease, Medical Primate Research Center, Kunming 650118, China*
[d]*Department of Lung Cancer Center and Center for Preclinical Safety Evaluation of Drugs, West China Hospital, Sichuan University, Chengdu 610041, China*

Received 8 May 2025; received in revised form 14 September 2025; accepted 16 October 2025

KEY WORDS

Syndrome coronavirus 2 (SARS-CoV-2);
Fusion protein;
Immunization;
Common binding region;
Conserve region;
Protection

Abstract COVID-19 and its variants have spread around the world, triggering a range of long-term sequelae and leading to the need for broadly effective vaccines. We have established a new fusion protein combining the receptor-binding domain region (SF2) and a newly identified conserved binding region (SF5) from the spike of SARS-CoV-2. This fusion protein (COVID19-SF2+SF5) specifically bound to VERO-E6 cells with higher efficiency than either region alone. Antibodies raised in mice against COVID19-SF2+SF5 cross-reacted with every fragment of SARS-CoV-2 and SARS. Additionally, antibodies against the fusion protein effectively neutralize pseudoviruses of both wild-type and mutant strains of SARS-CoV-2 (including BA.3, XBB.1.5, and EG.5), as well as SARS pseudoviruses. Protein interaction prediction and binding affinity determination revealed that the fusion protein exhibits strong binding capacity to three key host molecules: heparan sulfate proteoglycan (HSPG), neuropilin-1 (NRP1), and cluster of differentiation 147 (CD147). Analysis of representative viruses from four coronavirus genera (α, β, γ,

*Corresponding authors.
E-mail addresses: qinmeng212@scu.edu.cn (Meng Qin), hzl@imbcams.com.cn (Zhanlong He), yjiang@biopharmagen.com (Yongping Jiang).
Peer review under the responsibility of Chinese Pharmaceutical Association and Institute of Materia Medica, Chinese Academy of Medical Sciences.

https://doi.org/10.1016/j.apsb.2025.11.027

δ)—including 229E, NL63, OC43, HKU1, SARS-CoV, MERS-CoV, HKU20, and IBV—revealed that these coronaviruses share sequence similarity mainly on SF2 and SF5 regions. Furthermore, immunization of female hamsters with COVID19-SF2+SF5 provided significant protection against a SARS-CoV-2 virus challenge. Taken together, our results indicate that vaccination with a protein containing both an receptor binding domain (RBD) region and a common binding region provides strong protection during infection, thus suggesting a potential strategy to avoid evasion of host immune recognition by virus variants. Significantly, the observation that COVID19-SF2+SF5 immunization possesses stronger activity in reducing viral load at early stages suggests that the SF5 region might play an important role in virus recognition and binding to host cells. Based on these findings, we conclude that it is possible to develop universal vaccines and neutralizing monoclonal antibodies to curb the effects of mutations and to target multiple coronaviruses.

1. Introduction

As of 2025, severe acute respiratory syndrome coronavirus 2 (SARS-CoV-2) has infected over 800 million people globally, resulting in more than 8 million deaths, and has had a profound impact on public health systems worldwide[1]. COVID-19 has not only triggered an acute health crisis but has also led to a range of long-term sequelae, commonly referred to as "Long COVID", including persistent respiratory difficulties, myocardial injury, cognitive dysfunction, and mental health issues such as anxiety and depression. These long-term effects continue to burden patients' quality of life and healthcare infrastructure, underscoring the need for effective preventive strategies, particularly vaccines that mitigate infection risk[2-8]. Since SARS-CoV-2 emerged, remarkable progress has been achieved in vaccine development. Multiple platforms—including mRNA, adenoviral vector, inactivated virus, and recombinant protein vaccines—have received emergency use authorization or full approval, with over 150 candidate vaccines deployed globally[9-13]. These efforts have significantly curtailed SARS-CoV-2 transmission and reduced COVID-19 severity. Notable examples include protein subunit vaccines like ZF2001 and SCB-2019, which demonstrated 77.54% and 79.1% efficacy, respectively, against the Delta variant[14,15]. Nevertheless, several promising candidates remain stalled in development[10-13,16].

The ongoing emergence of immune-evasive variants, such as Omicron (B.1.1.529) and its sublineages (BA.4, BA.5), has diminished vaccine efficacy[17-28]. Consequently, SARS-CoV-2 vaccines now require annual updates, akin to seasonal influenza vaccines, to maintain effectiveness against circulating strains. For instance, updated versions of Comirnaty and Spikevax, targeting Omicron KP.2, were approved by the US Food and Drug Administration in August 2024—an achievement reflecting accelerated vaccine development timelines compared to traditional platforms[29,30].

Despite their overall safety, vaccines have been associated with rare adverse events, including myocarditis (linked primarily to mRNA vaccines) and thrombosis (associated with adenoviral vectors)[31]. These occurrences highlight the necessity for continued research to refine vaccine safety and efficacy against SARS-CoV-2 and future coronaviruses.

In response to rapid viral evolution and the threat of novel coronaviruses, global research has pivoted toward elucidating conserved mechanisms of viral entry and replication. Coronaviruses primarily infect cells *via* spike (S) protein binding to host receptors, with SARS-CoV-2 relying on the receptor binding domain (RBD) - angiotensin converting enzyme 2 (ACE2) interaction for entry.

Recent breakthroughs have identified prion-like domains (PLDs) within the RBD, which enhance infectivity and adaptive evolution through multivalent peptide−protein interactions[32]. Meanwhile, similar to human immunodeficiency virus (HIV), coronaviruses undergo conformational shifts during entry, exposing multiple binding sites that engage host co-receptors (*e.g.*, HSPG, CD147, NRP1) to facilitate membrane fusion[33-37]. Chinese research teams have pioneered the discovery of conserved binding motifs, enabling rational design of broad-spectrum antivirals targeting shared viral-host interaction networks[38]. For example, Dr. Yang Guang's[38] team reported the identification of a conserved hexapeptide core epitope (DVVNQN/Q) within the spike protein's RBD of coronaviruses, which is highly conserved across α/β/γ/δ coronavirus genera, mediates cross-viral neutralizing activity *via* a β-turn conformation, and whose critical role in the pre-fusion transition state of viral membrane fusion was elucidated using X-ray crystallography and cryo-electron microscopy, thereby providing a key target for the rational design of broad-spectrum antivirals.

Fusion protein vaccines, which combine key proteins from different coronaviruses, can stimulate a more comprehensive immune response and improve the broad-spectrum character and adaptability of vaccines to viral mutations[39]. SARS-CoV-2 shares genetic and structural similarities with other coronaviruses, such as SARS-CoV and MERS-CoV, providing a scientific basis for the development of fusion protein vaccines with broad activity. For example, combined SARS-CoV-2 and MERS-CoV vaccines have been proposed to combat viral variants[40], including a fusion protein consisting of fragments from parainfluenza virus-5 and MERS-S proteins, which has been developed as a candidate vaccine for COVID-19[41].

Our previous study utilized a structure-function approach to map the spike proteins of SARS-CoV-2 and SARS-CoV. We identified a novel cell-binding and cross-reacting region (COVID19-SF5) that is conserved in SARS-CoVs[42]. Building on this, we engineered a novel fusion protein (COVID19-SF2+SF5), which exhibited potent immunogenicity and conferred protective immunity against SARS-CoV-2 *in vitro* and in a hamster model.

2. Materials and methods

2.1. Oligonucleotides

The spike gene of SARS-CoV-2 was incorporated into plasmids sourced from Sangon Biotech, located in Shanghai, China. The

primers developed for the purpose of gene amplification were also produced by Sangon Biotech Co., Ltd., and their specifications can be found in Supporting Information Table S1.

2.2. Cell lines and pseudotyped virus

VERO-E6 cell lines were acquired from the Cell Resource Center of Shanghai Institutes for Biological Sciences, China. hACE2-293T cells were obtained from Delivectory Biosciences Inc. based in Beijing, China. Both cell lines were cultured in DMEM supplemented with 10% (*v*/*v*) fetal bovine serum (FBS), along with 100 U/mL penicillin and 100 mg/mL streptomycin, in a Thermo Fisher Scientific incubator set at 37 °C with 5% CO_2. The cells were subcultured on a regular basis. Furthermore, SARS-CoV-2 pseudovirus that expresses luciferase was purchased from Delivectory Biosciences Inc. (Beijing, China).

2.3. Viruses

The SARS-CoV-2 strain used in these studies was the Omicron strain (CCPM-B-V-049-2112-18). This study was performed as described previously in a biosafety level 3 (BSL3) laboratory following institutional biosafety guidelines by the Institute of Medical Biology, Chinese Academy of Medical Sciences. The P1 virus was subsequently passaged at a 1:1000 dilution on mycoplasma-free VERO-E6 cells (ATCC) in DMEM medium (supplemented with 1% penicillin/streptomycin) (Hyclone) and harvested when 80% cytopathic effect (CPE) became evident. The P2 virus stock was clarified by centrifugation at 6000×*g* for 5 min and stored at −80 °C until thawed for animal infections. The virus stock was titrated on Vero cells by conventional $TCID_{50}$ assay, as described previously[43].

2.4. Animals and ethics statement

Female BALB/c mice, aged 6 to 8 weeks, were obtained from the SLRC Laboratory Animal Center in Shanghai, China. The experimental protocols involving animals received approval from the Soochow University Animal Care and Use Committee (approval ID: 202404A0027). All procedures were conducted in accordance with the Guide for the Care and Use of Laboratory Animals established by Soochow University (China).

Female Syrian hamsters 5−6 weeks were purchased from Beijing Vital River Laboratory Animal Technology Co., China. The hamsters were randomly divided into various groups for subsequent experiments. All animal experiments were reviewed and approved by the Peking Union Medical College Animal Care and Use Committee (approval ID: DWSP202304001). At the conclusion of the experiments, euthanasia was conducted by administering ketamine/xylazine at a dosage of 100/10 mg/kg *via* intraperitoneal injection.

2.5. Plasmid construction

The sequences encoding COVID19-SF2 (amino acids 305-525), COVID19-SF5 (amino acids 880-1084), COVID19-SF6 (amino acids 1066−1237), and the combined COVID19-SF2+SF5 of SARS-CoV-2 were amplified using the designated primers. These sequences were engineered to include a His_6 tag at the C-terminus, along with specific restriction enzyme sites. After digestion with *Bam*H I and *Hind* III, the amplified fragments were inserted into the pQE-3 expression vector. The plasmids, designed to express fragments of the S subunit, were subsequently transformed into the *E. coli* M15 strain.

2.6. Protein expression and purification

The protein fragments were expressed as inclusion bodies. These inclusion bodies were harvested from lysates of IPTG-induced bacteria and dissolved in 6 mol/L guanidine hydrochloride. To purify the polyhistidine-tagged proteins, the Ni-NTA Purification System was utilized as outlined in prior methods[44]. Following purification, the proteins were diluted to 0.2 mg/mL in a sodium acetate buffer containing 8 mol/L urea (pH 5.4). Refolding of the proteins was achieved through a series of dialysis steps under optimized buffer conditions at 4 °C.

2.7. Flow cytometry analysis of protein fragments binding to cells

VERO-E6 cells were treated with 0.25% trypsin for digestion. Following this, 1.5×10^5 cells were incubated with His_6-tagged protein fragments at a concentration of 0.25 μmol/L for 1 h at 37 °C, excluding the control groups. Afterward, the cells were washed and stained with PE-conjugated anti-His-Tag antibody (Biolegend, San Diego, CA, USA) for 1 h at 4 °C. The cells were then washed again and resuspended for flow cytometry analysis. A total of 20,000 events were recorded for each sample using the BD FACSVerse™ system (Becton Dickinson, Franklin Lakes, NJ, USA). The data were analyzed using FlowJo software (Version 10.5.3, Tree Star Software, CA, USA), following previously established protocols [44-47].

2.8. Mouse immunization, sample collection, and purification

BALB/c mice aged 6−8 weeks ($n = 3$) were immunized by intramuscular (i.m.) injection with two doses spaced 14 days apart (Days 0 and 14) containing 0.1 mg of the fusion fragment of SARS-CoV-2 and Freund's complete or incomplete adjuvant. The mice received a boost dose with 0.1 mg of fusion protein without adjuvant on Day 28. Serum was collected 2 days after the last injection[44,48].

IgGs from serum specific to the fusion protein were purified using MabSelect™ PrismA (GE Healthcare), following the manufacturer's protocols. The concentration of the purified IgGs was evaluated using the Bio-Rad Bradford assay method.

2.9. Titer determination and cross-reaction of serum IgG by ELISA

The 96-well microtiter plates (Costar) were coated with 50 μL of protein fragments at a concentration of 2 μg/mL and incubated overnight at 4 °C. The plates were then washed with PBST and blocked using PBST with 1% BSA. Following this, diluted IgGs (ranging from 1:100 to 1:25,600) were added and incubated for 2 h at 37 °C. After washing, goat anti-mouse IgG HRP-conjugated antibody (Sangon Biotech, diluted 1:10,000) was added and incubated for 1 h at 37 °C. The plates were washed three more times, and the color reaction was developed using 3,3′,5,5′-tetramethylbiphenyldiamine (TMB) substrate. After a 15-min incubation, the reaction was halted with a 2 mol/L H_2SO_4

stop solution. Absorbance readings at 450 nm were taken using a Thermo microplate reader.

To assess cross-reactivity, the plates were coated with the fragments at equivalent molar concentrations (10 pmol/well). IgG was then added at a concentration of 0.05 μg/mL. All other procedures followed the same protocol as described previously.

The evaluation of female hamster serum samples for total IgG antibody responses was conducted in a manner analogous to the previously described protocol. The four corresponding protein fragments were diluted with 0.1 mol/L (8.4 g/L) $NaHCO_3$ to achieve a final concentration of 100 pmol/mL. A volume of 100 μL from the diluted protein solution was dispensed into each well of a 96-well plate and incubated overnight at 4 °C for coating. Subsequent procedures were followed as outlined earlier. The IgG titer for the female hamster protein fragments was determined by calculating the reciprocal of the highest serum dilution that yielded an average mean OD_{405} value $\geq$ 0.1 after background subtraction.

2.10. Pseudovirus neutralization assay for different strains of SARS-CoV and SARS-CoV-2

One day before the experiment, seed hACE2-293T cells to be infected into a 96-well cell culture plate at a density of approximately 2×10^4 cells/well. Pseudovirus infection will be performed the next day. Dilute the COVID19-SF2+SF5 IgG antibody with complete medium to a concentration of 20 μg/mL. Prepare a double-concentration pseudovirus solution using an appropriate inoculum titer determined from preliminary experiments. Mix the antibody solution and pseudovirus solution in equal volumes to prepare a mixed solution containing 10 μg/mL antibody and the pseudovirus concentration determined from preliminary experiments. Aspirate the supernatant medium using a multichannel pipette. Add 100 μL of the diluted pseudovirus-antibody mixture to the pre-seeded 96-well plate. After 6 h of treatment, replace with fresh complete medium and continue culturing for 48 h. At 48 h after medium replacement following pseudovirus infection, determine the antibody neutralization efficiency by Luciferase Assay Kit on a microplate reader. Finally, the inhibition rate was calculated based on the luciferase activity values obtained from the luciferase assay. The formula was calculating according to Eq. (1):

Inhibition rate (%) = [1−(Luciferase activity of experimental group−Luciferase activity of blank control)/(Luciferase activity of negative control−Luciferase activity of blank control)] × 100 (1).

2.11. Protein−protein docking analysis

To investigate the molecular interactions between the SARS-CoV-2 spike protein (S protein), fusion protein (SF2+SF5), and host receptors (ACE2, HSPG, NRP1, and CD147), a computational protein−protein docking approach was employed. First, the amino acid sequences of ACE2, HSPG, and NRP1 were retrieved from the UniProt database (Q9BYF1, P98160, O14786, and P35613). The three-dimensional (3D) structures of these proteins were predicted using AlphaFold3, a state-of-the-art deep learning-based protein structure prediction tool.

Subsequently, protein−protein docking was performed using the Vakser Lab protein docking server, which utilizes a geometric recognition algorithm to predict binding interfaces and orientations. The spike protein and COVID19-SF2+SF5 were docked with ACE2, HSPG, NRP1, and CD147, respectively. The docking simulations were conducted under default parameters, and the top 10 docking poses were selected based on the lowest binding energy scores.

Finally, the docking results were visualized and analyzed using PyMOL (version 2.5.2). The binding interfaces and key residues involved in the interactions were identified. The binding free energy (ΔG) of each complex was calculated using the PDBePISA server (https://www.ebi.ac.uk/pdbe/pisa/), which provides a comprehensive analysis of protein−protein interactions, including interface area, hydrogen bonds, and binding energy. Statistical analysis was performed to compare the binding affinities between the spike protein and COVID19-SF2+SF5 protein with the host receptors.

2.12. Determination of the binding between the COVID19-SF2+SF5 protein and ACE2, HSPG, NRP1, and CD147 by ELISA

The 96-well microtiter plates (Costar) were coated with 100 μL of each of ACE2, HSPG, NRP1, and CD147 at a concentration of 0.5 μg/mL and incubated overnight at 4 °C. The plates were then washed with PBST and blocked using PBST with 1% BSA. Following this, COVID19-SF2+SF5 protein (ranging from 0.336 nmol/L to 5.25 μmol/L) were added and incubated for 1 h at 37 °C. After washing, COVID19-SF2+SF5 IgG (2 μg/mL) was added and incubated for 1 h at 37 °C. After washing, goat anti-mouse IgG HRP-conjugated antibody (Sangon Biotech, diluted 1:10,000) was added and incubated for 1 h at 37 °C. The plates were washed three more times, and the color reaction was developed using 3,3′,5,5′-tetramethylbiphenyldiamine (TMB) substrate. After a 15-min incubation, the reaction was halted with a 2 mol/L H_2SO_4 stop solution. Absorbance readings at 450 nm were taken using a Thermo microplate reader. Finally, the data were fitted to a curve, and the dissociation constant (K_D) was calculated.

2.13. Syrian hamsters challenge

Female Syrian hamsters used in these studies were supplied by a breeding colony at Shouke Lingfu (Beijing) Bio-technology Co., (China) in a pathogen-free facility. All the Syrian hamsters were acclimated for a minimum of one week prior to the initiation of experimental procedures. Syrian hamsters were randomly assigned to their respective groups and housed in a temperature-controlled, light-cycled facility. Syrian hamsters were supplied with food and water ad libitum and were monitored daily throughout the course of the experiments.

Firstly, female Syrian hamsters were immunized by intramuscular (i.m.) injection with four doses spaced 14 days apart (Days 1 to 42) containing 0.1 mg of fusion fragment and 0.1 mL Imject™ Alum Adjuvant, and IgG titers were measured every 7 days. Then twelve-week-old female Syrian hamsters were infected with 2×10^4 $TCID_{50}$ of SARS-CoV-2 (Omicron variant) by an intranasal route (i.n.) of administration in a 50 μL volume. Blinding of the animal experiments was not performed.

2.14. Pharyngeal swabs, blood, lung, lung lymph and brain tissues collection

Pharyngeal swab samples were collected in DMEM containing P/S daily, starting one day before inoculation. The collected pharyngeal swab samples were diluted 1:1 by volume and aliquoted for quantitative real-time RT-PCR.

All female Syrian hamsters were exsanguinated *via* cardiac puncture under deep isoflurane anesthesia prior to euthanization. Whole blood and serum were collected in Becton, Dickinson and Company (BD, USA) microtainer tubes (K2-EDTA or serum, respectively), as per the manufacturer's instructions. After euthanization, lung tissues were collected. Part of lung tissue was used to prepare lung tissue homogenate, determine its viral load and test for viral $TCID_{50}$. Another part of lung tissue was fixed in 4% paraformaldehyde. Harvested tissue sample (lung, pulmonary lymph, and brain) for infectious assays were flash-frozen and stored at −80 °C until later use.

2.15. Viral load determination by quantitative real-time RT-PCR

SARS-CoV-2 viral RNA in lung and nasal tissues from challenged hamsters was detected by quantitative reverse transcription PCR (RT-qPCR). Briefly, the lung and nose tissues were weighed and homogenized with Trizol, and virus RNA could be isolated according to the manufacturer's protocol.

For quantification, a single-tube One Step TB Green PrimeScript TM PLUS RT-PCR Kit (Perfect Real Time, Takara, Japan) and a 7500 Fast Real-Time RT-PCR System (Ap-plied Biosystems, Foster City, CA, USA) were used. The reaction solution consisted of the following: 10 μL of 2 × One Step TB Green RT-PCR Buffer, 1.2 μL of TaKaRa Ex Taq HS Mix, 0.4 μL of PrimeScript PLUS RTase Mix, 0.8 μL of PCR Forward Primer (10 μmol/L), 0.8 μL of PCR Reverse Primer (10 μmol/L), 2 μL of Total RNA, 4.8 μL of RNase Free dH2O, resulting in a total reaction volume of 20 μL. Real-time PCR was performed under the following conditions: step1 and 2 at 42 °C for 5 min, 95 °C for 10 s; step3 at Reps: 40, 95 °C for 5 s, 60 °C for 30 s. And one sets of primers and probes was used to detect a region of the ORF1a/b of the viral genome of SARS-CoV-2, with sequences as follows: ORF1a/b-F, CCCTGTGGGTTTTACACTTAA; ORF1a/b-R, ACG ATTGTGCATCAGCTGA; ORF1a/b-probe, FAM-CCGTCTGCG GTATGTGGAAAGGTTATGG-BHQ1. Viral RNA levels in lung and nose tissues were expressed as ORF1a/b gene copy numbers per milligram after comparison with a standard curve produced using serial ten-fold dilutions of SARS-CoV-2 RNA[49,50].

2.16. Cytopathic effect (CPE) assay

Lung tissues from hamsters were weighed and homogenized in 1 mL of DMEM medium (supplemented with 1% penicillin/streptomycin). Virus titrations were per-formed using endpoint titration in Vero cells, which were inoculated with 10-fold serial dilutions of the tissue homogenates in 96-well plates (100 μL/well). The titrating tissue homogenate was added to 100 μL of Vero cell suspension (DMEM with 4% FBS and 2% penicillin/streptomycin, 2×10^5 cells/mL) in each well, and the mixture was incubated at 37 °C with 5% CO_2. Cytopathic effect was assessed 6 days later.

2.17. Immunohistochemistry

Paraffin-embedded sections were de-paraffinized using xylene, rehydrated in graded ethanol, and deionized water. Sections were subjected to antigen retrieval treatment by boiling in acidic pH citrate buffer (Vector Laboratories) for 20 min in a steam cooker. 3% hydrogen peroxide in methanol was used to block the endogenous peroxidase for 20 min and washed with 1 × PBS two times, followed by blocking with horse serum (Vector Lab) for 30 min at room temperature. Sections were treated with ACE2 antibody (#MA5-32307, 1:200 or #AF933; 2 μg/mL) overnight in a humidified chamber at 4 °C. Sections were washed twice with 1X PBS for 5 min each. In MA5-32307 antibody case, slides were treated with horse anti-rabbit/mouse IgG biotinylated universal antibody (Vector Laboratories) for 45 min at room temperature and with ABC reagent for 30 min. For AF933 antibody, the slides were incubated with Goat IgG VisUCyte HRP Polymer (#VC004, R&D Systems) and incubated for 45 min at room temperature (without ABC incubation). The stain was developed using 3,3′-diaminobenzidine (DAB; Vector Laboratories) as a substrate according to the manufacturer's instructions, with hematoxylin used as a counter-stain. Sections were dehydrated with ethanol, cleared with xylene, and mounted with Vecta mount permanent mounting medium. Then they were observed under the microscope (Leica ICC500), and images were captured at × 40 magnification.

2.18. Statistical analysis

The results are expressed as mean ± standard deviation (SD) derived from a minimum of three independent experiments, each involving duplicate samples. Statistical differences were assessed using one-way analysis of variance unless otherwise specified. A *P*-value of less than 0.05 was regarded as statistically significant. For experimental data involving dose-response relationships (*e.g.*, antibody binding affinity assays), they were fitted to a sigmoidal curve to better characterize the gradual saturation or progressive change trends of the measured indicators. Graphical representations were created utilizing GraphPad Prism (version 8.0; GraphPad, La Jolla, CA, USA) and Microsoft Excel.

3. Results

3.1. Production of a COVID19-SF2+SF5 recombinant fusion protein

In previous studies, we described the construction of six recombinant proteins containing fragments of the SARS-CoV-2 spike protein (named COVID19-SF1 through COVID19-SF6) and six recombinant proteins containing fragments of the SARS-CoV spike protein (named SARS-SF1 through SARS-SF6). As depicted in Fig. 1A and B, COVID19-SF2 contains the RBD of the SARS-CoV-2 spike protein, and COVID19-SF5 strongly cross-reacted with antibodies directed against all twelve recombinant S protein subunit fragments, implying that COVID19-SF5 shares common antigenicity with the S subunit proteins of both SARS-CoV-2 and SARS-CoV. Therefore, a new fusion protein was created that includes both the COVID19-SF2 and SF5 fragments connected by a flexible linker peptide, Gly_4Ser (COVID19-SF2+SF5). A plasmid directing the expression of this fusion protein which has a His_6-tag at the C-terminus was constructed by double digestion with the restriction enzymes *Bam*H I and *Nco* I and then verified by sequencing. The recombinant protein was expressed in *E. coli* and purified under denaturing conditions by affinity chromatography with Ni-NTA resin. The refolded protein was recovered with high purity (Fig. 1D).

Flow cytometry analysis using PE-conjugated anti-His-tag antibody demonstrated differential binding of the fusion proteins to SARS-CoV-2-susceptible VERO-E6 cells. As shown in Fig. 1C,

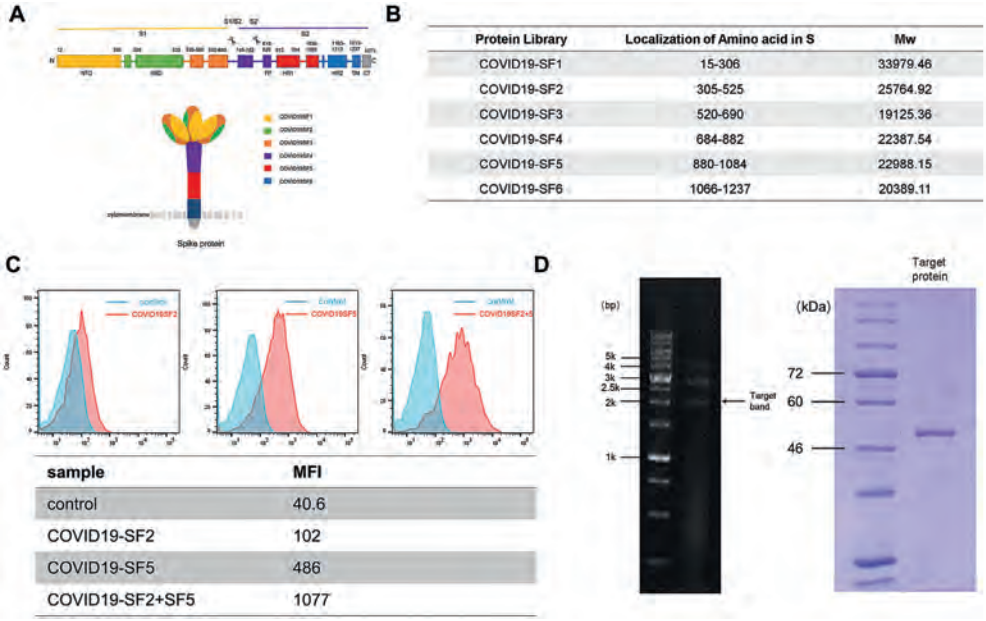

Protein Library	Localization of Amino acid in S	Mw
COVID19-SF1	15-306	33979.46
COVID19-SF2	305-525	25764.92
COVID19-SF3	520-690	19125.36
COVID19-SF4	684-882	22387.54
COVID19-SF5	880-1084	22988.15
COVID19-SF6	1066-1237	20389.11

sample	MFI
control	40.6
COVID19-SF2	102
COVID19-SF5	486
COVID19-SF2+SF5	1077

Figure 1 Recombinant fusion protein production and cell-binding ability. (A) Structural features of the SARS-CoV-2 spike protein and the flow chart of protein library construction. The listed domain boundaries are the NTD, N-terminal domain; RBD, receptor-binding domain; FP, fusion peptide; HR1, heptad repeat 1; HR2, heptad repeat 2; TM, transmembrane domain; and CT, cytoplasmic tail. For visual clarity, box lengths are not to scale. (B) Amino acid locations and molecular weights of the protein fragments. (C) Flow cytometry was performed to assess the binding activity of the fusion protein to VERO-E6 cells. Cells were incubated with 0.25 μmol/L His_6-tagged COVID19-SF2, COVID19-SF5, or COVID19-SF2+SF5. The blue curve represents the cells without added protein. The red curves represent fragment binding. (D) The plasmid encoding the fusion protein was verified by agarose gel electrophoresis following digestion with *Bam*H I and *Nco* I. Expression and purification of the protein fragment were analyzed by SDS-PAGE.

COVID19-SF2 showed minimal interaction (MFI = 102), whereas COVID19-SF5 exhibited 3.76-fold stronger binding signal (MFI = 486), suggesting broader receptor engagement. The combined COVID19-SF2+SF5 fusion protein displayed superior binding activity (MFI = 1077), with a >10-fold MFI increase over SF2 and 2-fold enhancement *versus* SF5, indicating synergistic effects between the two fragments.

3.2. Evaluation of mouse antibodies raised against the fusion protein

To investigate the ability of the COVID19-SF2+SF5 fusion protein to induce an effective immune response, Balb/C mice were immunized with the protein fragment (Fig. 2A), and total IgG was purified from the resulting antisera with protein G Sepharose. The pooled IgG sample was diluted to 50 μg/mL. The titer of this pooled sample against the fusion subunit fragment was determined to be approximately 1:1600 by ELISA, suggesting that the fusion protein is strongly immunoreactive.

The cross-reactivity of the IgG against 12 protein fragments from the SARS-CoV-2 S subunits was determined (Fig. 2B). In this analysis, antibodies raised against the fusion protein cross-reacted with each S protein fragment with generally strong binding affinities. Thus, exposure to the fusion protein led to the production of highly specific antibodies that interact with a common region of SARS-CoVs.

Pseudovirus neutralization experiments were further conducted on various SARS-CoVs, including SARS-CoV-1 and wild-type or mutant strains of SARS-CoV-2 (BA.3, XBB.1.5, and EG.5). The results showed that the IgG of the fusion protein inhibited infections by both wild-type and mutant strains in a dose-dependent manner. Although RBD-targeting neutralizing antibodies exhibited a strong inhibitory effect against SARS-CoV-2 (inhibition rate >90%), their inhibitory effect on SARS-CoV-2 mutant strains was significantly lower than that of the fusion protein IgG at high concentrations (with inhibition rates ranging from 65.6% to 77.8%). Additionally, high-concentration fusion protein IgG also showed a significant inhibitory effect on SARS-CoV-1 (inhibition rate ∼48%, Fig. 2C).

Furthermore, sequence alignment of representative spike proteins from viruses across the four genera of the Coronaviridae family, including 229E and NL63 coronaviruses (Genus α); SARS-CoV, MERS-CoV, OC43 coronavirus, and HKU1 coronavirus (Genus β); HKU20 coronavirus (Genus γ); and IBV (Genus δ), revealed that the regions where these viruses share identical or similar amino acid sequences with SARS-CoV-2 are primarily concentrated in two segments: the 200−500 amino acid region and the 600−1200 amino acid region. These two regions correspond precisely to the SF2 and SF5 regions of the SARS-CoV-2 spike protein, respectively, and together account for more than one-third of the total number of similar amino acids shared between these coronaviruses and SARS-CoV-2 (Fig. 2D, Supporting Information Tables S2−S4). These findings indicate that the novel fusion protein, which targets these common conserved binding sites, could serve as a potential vaccine candidate against β-coronaviruses, and even the entire Coronaviridae family.

3.3. Fusion protein exhibits high potential to bind HSPG, NRP1 and CD147 receptors, while binding to ACE2

Currently, the mechanism by which SARS-CoV-2 enters cells has predominantly been centered around the binding of the spike

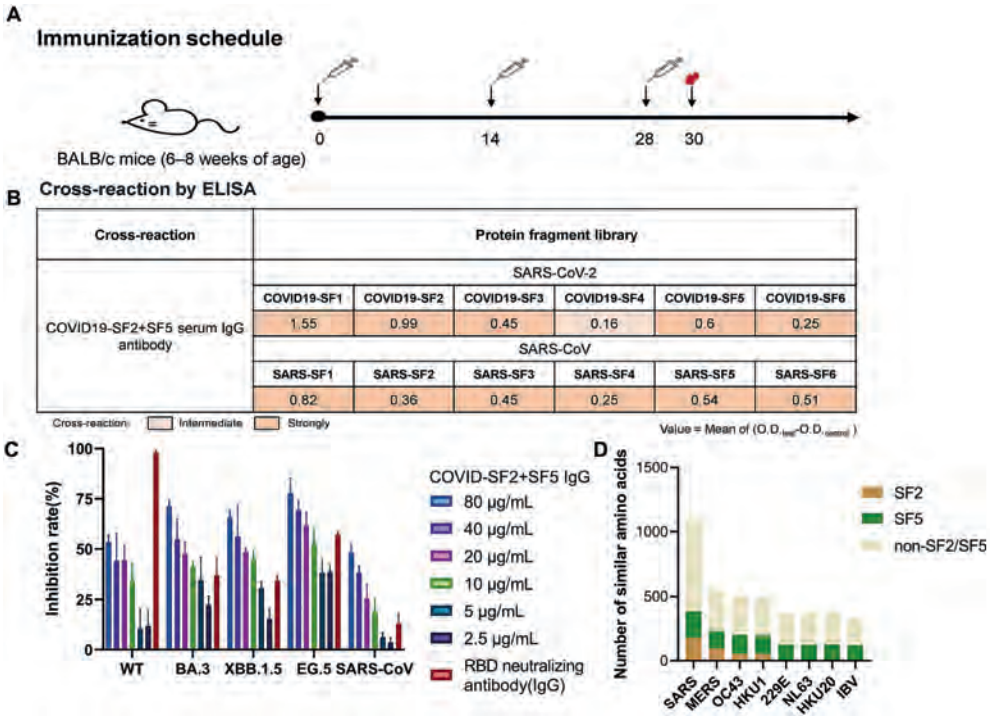

Figure 2 Cross-reaction of antibodies raised against COVID19-SF2+SF5 with other SARS-CoV proteins. (A) Mouse immunization schedule. (B) ELISA was used to test interaction of COVID19-SF2+SF5-specific IgG (0.05 μg/mL) against 12 protein fragments (10 pmol/well) from SARS-CoV and SARS-CoV-2. Deep pink indicates a strong reaction ($OD_{test}-OD_{control} > 0.2$), light pink indicates an intermediate reaction ($0.1 < OD_{test}-OD_{control} < 0.2$). Mean values of three ELISA replicates are shown. (C) Pseudovirus neutralization experiments of fusion protein antibodies at different concentrations against SARS and SARS-CoV-2 (wild-type, BA.3, XBB.1.5, and EG.5). (D) The number of similar amino acids from the spike protein sequence alignment between different coronaviruses and SARS-CoV-2.

protein to the ACE2 receptor on the cell membrane. However, emerging evidence from previous studies has reported that other receptors[48-50], including HSPG, NRP1, CD147, AXL, and SR-B1, also play significant roles in facilitating spike protein binding and viral infection[34-36].

Through protein−protein docking analysis, we quantified the binding affinities of the SARS-CoV-2 spike protein (Supporting Information Fig. S1). The results showed that the spike protein has a binding energy of −20.8 kcal/mol with ACE2, while its binding energies with HSPG, NRP1, and CD147 are −14.5, −17.2, and −11.8 kcal/mol, respectively (Table 1). Furthermore, the binding interactions were visualized, with a particular focus on magnifying the binding sites in the SF2/SF5 regions (Fig. 3A, C, E and G). Except for ACE2, approximately one-third of the binding sites between the spike protein and ACE2 are located in the SF2/SF5 regions; while for the HSPG, NRP1, and CD147 proteins, most of their binding sites with the spike protein are located in the SF2/SF5 regions (Supporting Information Tables S6−S8). Images and data related to AXL and SR-B1 proteins have been supplemented in Supporting Information Figs. S2 and S3, Tables S5, S9, and S10. These negative binding energies, especially their relatively high absolute values, fully indicate that there is a strong binding potential between the spike protein and these alternative receptors.

Based on the above findings, we further examined the binding ability of the COVID19-SF2+SF5 to HSPG, NRP1, and CD147 proteins. Protein−protein docking analyses determined that the binding energies of the COVID19-SF2+SF5 with HSPG, NRP1, and CD147 were −31.0, −24.7, and −3.1 kcal/mol, respectively (Table 1). In ELISA experiments, COVID19-SF2+SF5 at varying concentrations (ranging from 0.336 nmol/L to 5.25 μmol/L) were incubated with these receptors. Results showed that the K_D of the COVID19-SF2+SF5 with ACE2 was 99 ± 8.1 nmol/L, with HSPG was 153 ± 7.9 nmol/L, with NRP1 was 118 ± 17.9 nmol/L, and with CD147 was 160 ± 23.3 nmol/L (Fig. 3B, D, F, and H). Combining the outcomes of protein−protein docking analyses and ELISA experiments, these results demonstrate that the receptor proteins HSPG, NRP1, and CD147, like ACE2, possess favorable binding ability to the fusion protein.

Collectively, these findings indicate that SARS-CoV-2 does not rely solely on ACE2 for cellular entry. Instead, it can interact with alternative receptors such as HSPG, NRP1, and CD147, thereby expanding the spectrum of potential routes for viral entry into host cells. By fusing SF2 and SF5—key components of the S1 and S2 subunits, respectively, the fusion protein exhibited strong binding

Table 1 Affinity of spike protein and COVID19-SF2+SF5 to ACE2, HSPG, NRP1, and CD147.

Protein A	Protein B	Affinity (kcal/mol)
Spike protein	ACE2	−20.8
	HSPG	−14.5
	NRP1	−17.2
	CD147	−11.8
COVID19-SF2+SF5	ACE2	−8.9
	HSPG	−31.0
	NRP1	−24.7
	CD147	−3.1

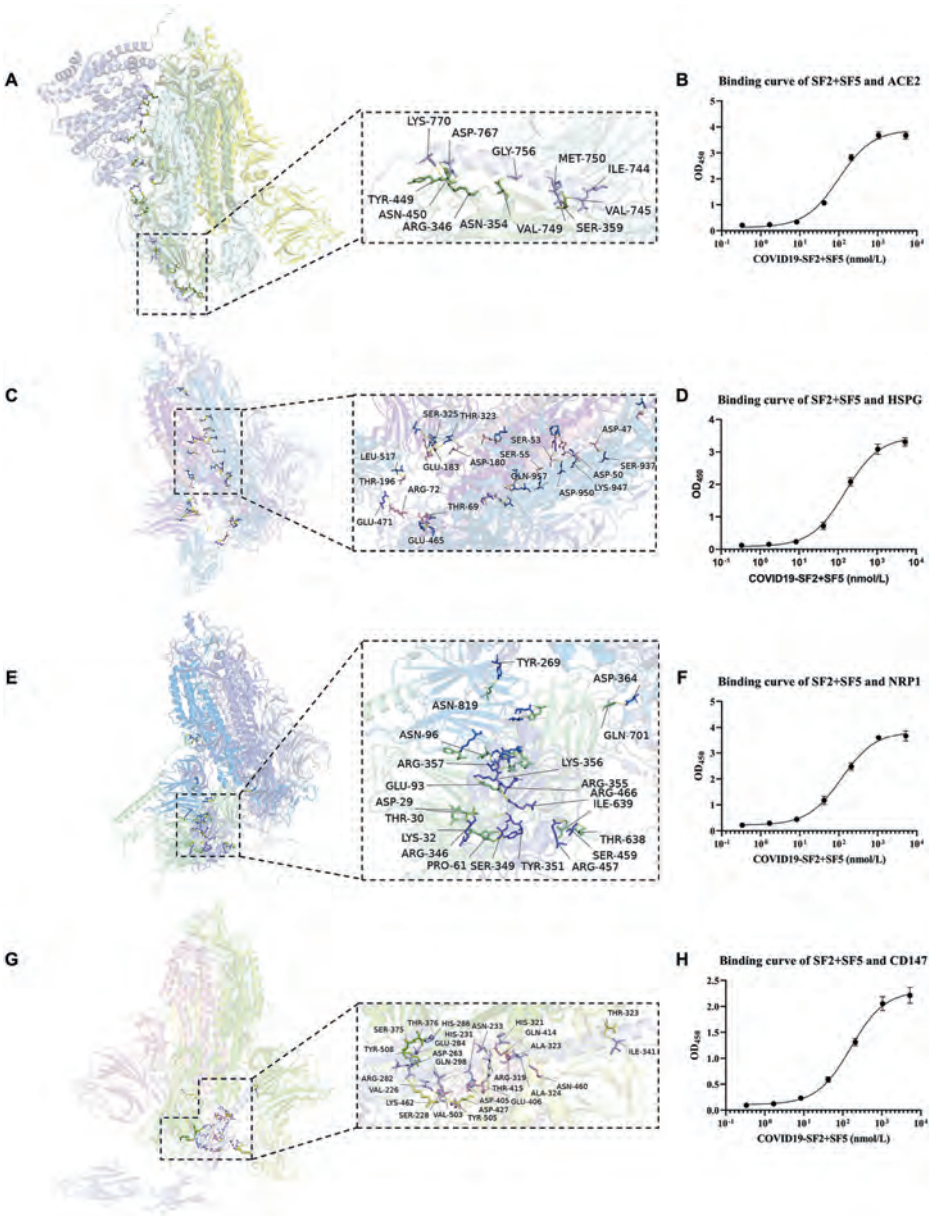

Figure 3 Docking prediction between the spike protein and different receptor proteins, and ELISA binding assay between different receptor proteins and the COVID19-SF2+SF5. (A) Spike protein binding to ACE2 (Magnify the binding sites in the SF2/SF5 regions). (B) Binding curve of COVID19-SF2+SF5 with ACE2. (C) Spike protein binding to HSPG (Magnify the binding sites in the SF2/SF5 regions). (D) Binding curve of COVID19-SF2+SF5 with HSPG. (E) Spike protein binding to NRP1 (Magnify the binding sites in the SF2/SF5 regions). (F) Binding curve of COVID19-SF2+SF5 with NRP1. (G) Spike protein binding to CD147 (Magnify the binding sites in the SF2/SF5 regions). (H) Binding curve of COVID19-SF2+SF5 with CD147.

affinity to both ACE2 and other host receptors. We hypothesize that antibodies targeting this novel fusion protein could simultaneously block multiple viral entry and fusion pathways, offering a more comprehensive and effective defense strategy against the coronaviruses.

3.4. Immunogenicity in a Syrian hamster model

Because of the success of the fusion protein in raising an immune response in mice, we further evaluated the vaccine activity of the protein in a Syrian hamster model. We employed a prime-boost regimen with four protein fragments, COVID19-SF2, COVID19-SF5, COVID19-SF6, or COVID19-SF2+SF5, along with PBS as a control. Inoculations were performed on Days 0, 14, 28, and 42 (Fig. 4A). No adverse effects or clinical signs were observed as a result of vaccination with any of the fragments.

Weekly serum samples collected from the hamsters were tested for the presence of specific antibodies using ELISA (Fig. 4A). Antibodies were detectable as early as one week after the first immunization. The titer reached a plateau on Day 14 of the protocol, and this level remained essentially constant until the final

immunization on Day 42 (Fig. 4B). Eight days after the fourth immunization (Day 50), the antibody titers were comparable among the four protein fragments (Fig. 4C).

3.5. Protection against viral infection in a Syrian hamster model

The female hamsters that had been inoculated four times with PBS, COVID19-SF2, COVID19-SF5, COVID19-SF6 or COVID19-SF2+SF5 were challenged with SARS-CoV-2 (Omicron strain) one-week post-immunization (Fig. 4A). The animals were followed by 4-day pharyngeal swab collections before sacrifice and histopathological evaluation. Pharyngeal swabs were collected daily on Day 1 through 4 days post-infection (dpi) and were titrated for viral RNA (vRNA) to detect viral shedding in the upper respiratory tract.

The viral load and pathological changes were reduced in female hamsters vaccinated with COVID19-SF2+SF5. Throat viral loads in throat swabs from the SF2+SF5 group were significantly lower than those in the PBS group at dpi2. While a transient increase was observed at dpi3, the viral load decreased again at dpi4 (Fig. 5A). These results indicate that SF2+SF5 can inhibit viral infection at the early stage, preventing high-level viral loads. The nucleic acid load in the nasal cavity increased at first and then decreased, but there was no significant difference among the groups (Fig. 5C).

Among the organs tested, the vRNA load was highest in lung tissue, followed by lung lymph and brain tissue, and a small amount of vRNA was detected in blood after 4 days post-infection (dpi). Compared to control animals, the vRNA load in brain tissue of hamsters treated with COVID19-SF2 was significantly reduced, and the loads in the lung tissue of hamsters treated with COVID19-SF2 or COVID19-SF2+SF5 were also significantly reduced (Fig. 5B). The results of $TCID_{50}$ analyses were consistent with the viral load results based on vRNA; here, hamsters inoculated with COVID19-SF2 or COVID19-SF2+SF5 had significantly lower viral loads in lung tissue compared to control animals (Fig. 5D).

As illustrated in Fig. 6, the severity of pathological findings was concordant with the amount of virus in the lung. On dpi4, inflammatory cell infiltration (red arrow), alveolar wall thickening (black arrow), and alveolar collapse with pink edema (blue arrow) were observed in the lungs of hamsters inoculated with PBS, COVID19-SF5, or COVID19-SF6. Conversely, the pathological changes were mild and the lung tissue construction remained nearly normal in hamsters inoculated with COVID19-SF2 or COVID19-SF2+SF5. Taken together, these results indicated that immunization of hamsters with COVID19-SF2+SF5 provided significant protection against a SARS-CoV-2 virus challenge.

4. Discussion

With the end of the COVID-19 pandemic emergency, the global COVID-19 vaccine research and development field has shown new characteristics. The direction of COVID-19 vaccine research and development shift to focus on innovation, with more attention paid to the broad-spectrum and long-term effects of vaccines, in preventing and resolving major epidemics and major public health emergencies in the future.

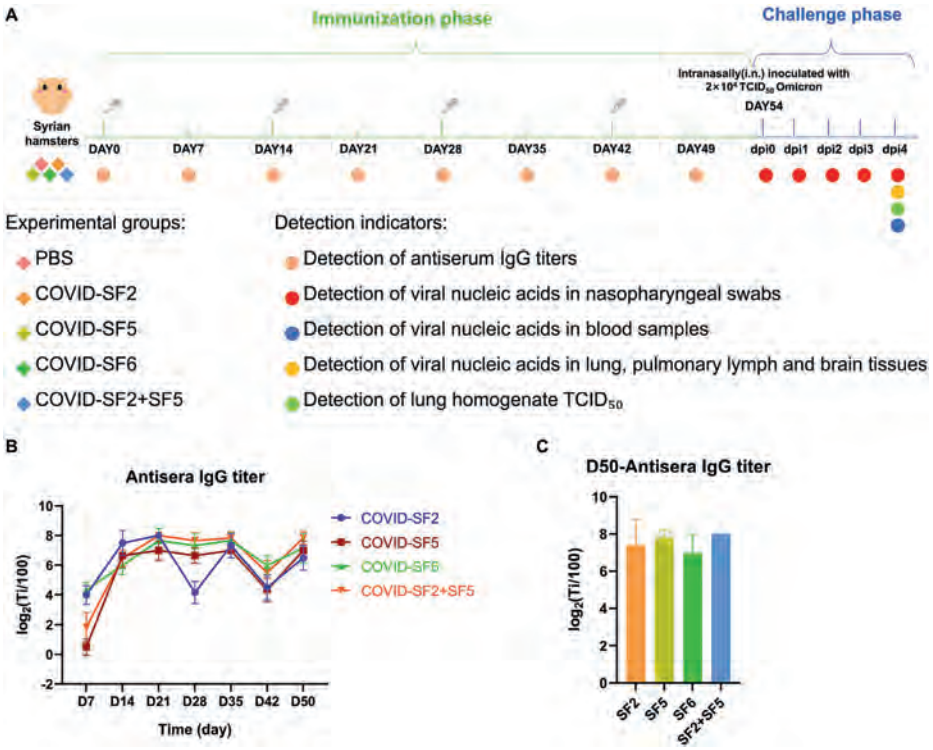

Figure 4 Experimental design and antibody responses to vaccination in Syrian hamsters. (A) Adult female Syrian hamsters ($n = 5$) were vaccinated with COVID19-SF2, COVID19-SF5, COVID19-SF6, COVID19-SF2+SF5, or PBS on Days 0, 14, 28, and 42, with blood collection performed weekly until Day 50. (B) Sera from collected blood samples were tested for antibody response at each week for 6 weeks and on Day 8 post challenge. (C) Sera from collected blood samples were tested for antibody response on Day 50.

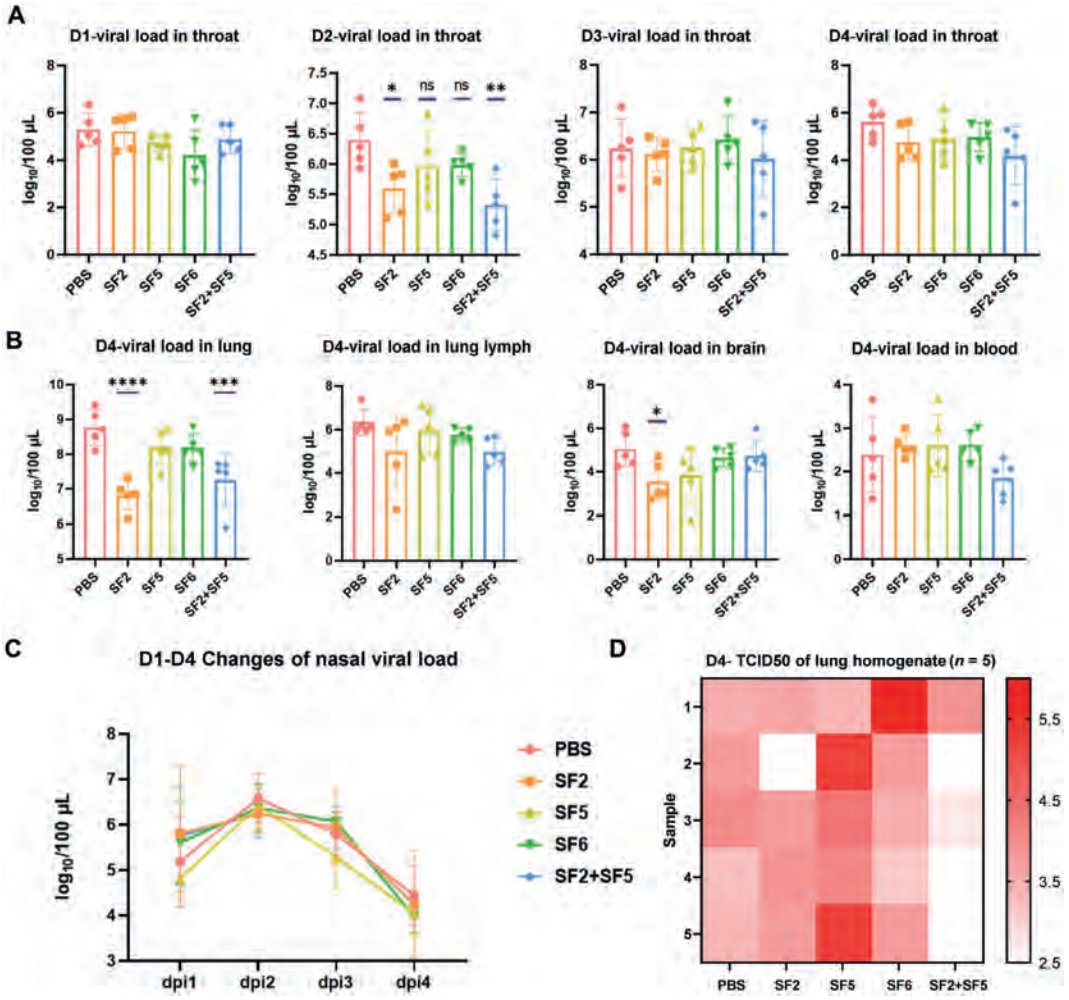

Figure 5 Efficacy of vaccination with the fragments in female Syrian hamsters. (A) Pharyngeal swabs were collected on 4 days post-infection (dpi) and titrated for virus RNA by qPCR. (B) On dpi4, total viral RNA from lung, lung lymph, brain, and blood were quantified by qPCR. (C) Changes to the nasal viral load over dpi1−dpi4 were quantified by qPCR. (D) Virus titers and copy numbers in lung homogenates were measured on dpi4. Data shown as mean values ($n = 5$); light to dark color indicates low to high virus titers. Data are presented as meas ±SD, $^{*}P < 0.05$, $^{**}P < 0.01$, $^{***}P < 0.001$, $^{****}P < 0.0001$. n.s., not significant.

Researchers have made great efforts in analyzing the viral structure as well as its infection and fusion mechanisms. Cryo-electron microscopy studies by various groups showed that there were at least two states of the trimeric S protein (open or closed) with RBDs in different states (standing or lying)[51]. Despite the traditional known ACE2 receptor binding approaches, TRMPSS2 binding[52], furin cleavage[53], pH[54], temperature[55], and other additional host factors[56], contributing to the transition from a closed conformation to an open conformation, and triggers virus entry and membrane fusion.

Recently, Eduardo Olmedillas and colleagues[57] have designed and characterized a pre-fusion-stabilized SARS-CoV-2 S2-only antigen, and a structural analysis demonstrated an open spike and potential "breathing adjustments". Specifically, anti-S2 antibodies isolated from humans, noting most epitope mapping focuses on S1, demonstrated cross-reaction for S1+S2, pre-fusion S2, post-fusion S2, etc., with 90% of S2 mAbs binding to XBB1.1 and SARS-CoV-1 spikes, highlighting the S1+S2 pre-fusion structure interaction and significance in virus entry. Moreover, similar conformation transition is also reported from other β-coronaviruses, including MERS, OC43, and HKU1[58-60].

In the present study, a fusion protein combining fragments COVID19-SF2, a well-established RBD, and COVID19-SF5, a newly discovered conserved binding region, was produced in *E. coli*. In the cell binding study, COVID19-SF2+SF5 demonstrated the enhanced binding toward VERO-E6 cells compared with the single domain proteins. Furthermore, cross-reaction of antiserum against COVID19-SF2+SF5 was observed with every protein fragment of SARS-CoV and SARS-CoV-2 in ELISA. Interestingly, COVID19-SF1 exhibited the strongest cross-reactivity with the IgGs of COVID19-SF2+SF5, likely attributable to its high molecular weight (~33 kDa) and the presence of conserved repeated binding domains in the spike protein. Pseudovirus neutralization assays demonstrated that the IgGs of COVID19-SF2+SF5 exerted significant inhibitory effects on multiple strains of both SARS-CoV and SARS-CoV-2 (including mutant strains). Furthermore, through sequence homology alignment analysis, we found that SF2 and SF5 are conserved

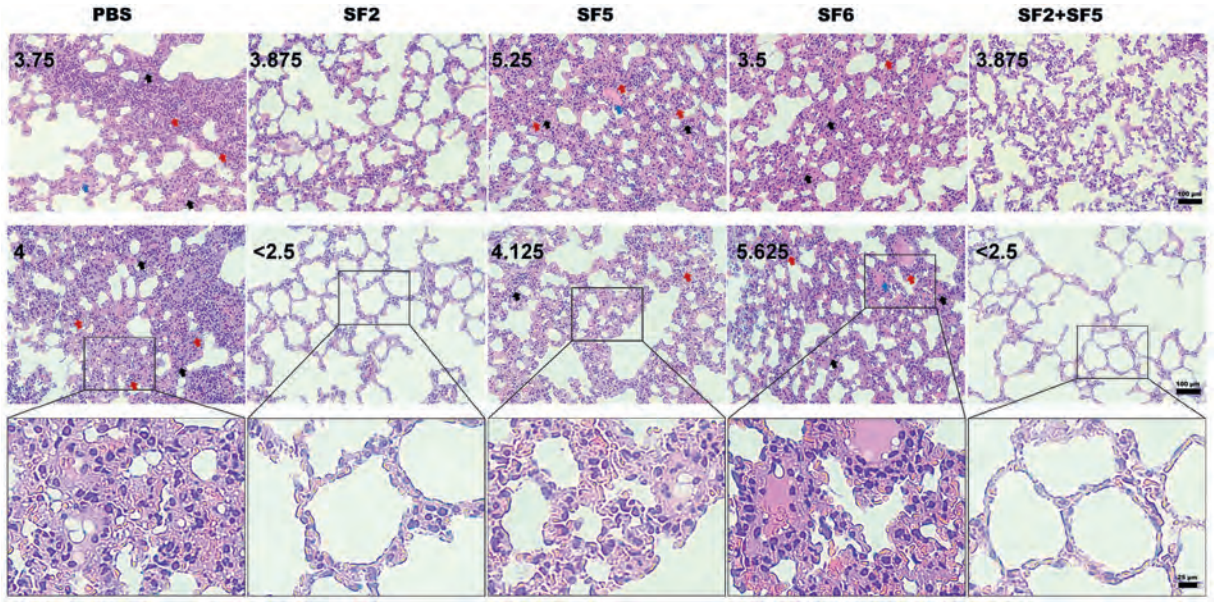

Figure 6 *In vivo* determination of protective activity of vaccination with fusion proteins. Lung tissues were harvested at 4 days post SARS-CoV-2 challenge from female hamsters that were previously vaccinated with PBS, COVID19-SF2, COVID19-SF5, COVID19-SF6, or COVID19-SF2+SF5. Formalin-fixed, paraffin-embedded lung tissues were stained with hematoxylin and eosin (H&E). The numbers on the slides are the $TCID_{50}$ values for the corresponding lung homogenate. The bottom panels are high-magnification images from a representative area of the middle panels. The scale bar represents 100 μm (top and middle panels) or 25 μm (bottom panels).

sequences sharing by various β-coronaviruses, which is also reported by other groups[61].

SARS-CoV-2 invade human cells mainly by using ACE2 to gain entry and initiate respiratory infection, but ACE2 alone may not be sufficient. HSPG, NRP1, CD147 and other co-receptors, were previously reported to interact directly with S protein to facilitate the entry of SARS-CoV-2 into human cells[34,56]. In this study, we first assessed the binding capacity of COVID19-SF2+SF5 to HSPG, NRP1, and CD147 using protein docking. Subsequently, specifical binding affinity of fusion protein with receptors were determined by ELISA. It was noted that COVID19-SF2+SF5 exhibits robust binding ability to these aforementioned receptor proteins. In hamster models, immunization with the fusion protein effectively reduced viral load at early stages with safety.

Although the results of this study reveal the broad-spectrum protective effect of the fusion protein against pseudoviruses of SARS-CoVs, further in-depth research is essential on its broad-spectrum protective ability against other β-coronaviruses including MERS, OC43, 229E, NL63, and HKU1. Meanwhile, more animal models should be continuously studied to address the limitations of limited animal protection. Additionally, other conserved regions except spike is validated to boost for T cell immunization and protection against β-CoVs[62], the follow-up study by combining both spike fusion protein and T cell enhanced regions can be further studied in the future.

5. Conclusions

In summary, we generated a new fusion protein combining the receptor binding domain region (SF2) and a newly identified conserved binding region (SF5) from the spike protein of SARS-CoV-2. In protein docking prediction and binding determination, it demonstrated strong binding affinity not only to ACE2, but also to host receptors including HSPG, NRP1, and CD147. In hamster models, immunization with the fusion protein effectively reduced viral load at early stages with safety. Thus, we propose that in addition to the RBD domain, the COVID19-SF5 region of the spike protein may facilitate viral conformational changes and play an important role in COVID19 fusion and entry. Based on these studies, fusion protein COVID19-SF2+SF5 can be developed for more effective SARS-CoVs vaccine to eliminate viral immune escape capabilities.

Acknowledgments

This work was supported by the Science and Technology Program of Suzhou, China (Su-2020-169), the National Key Research and Development Program of China (2024YFFO728801), the National Natural Science Foundation of China (52473137) and the 135 Project for Disciplines of Excellence of West China Hospital Sichuan University, China (ZYGD23011).

Author contributions

Yongping Jiang, Zhanlong He and Meng Qin conceived, designed, and supervised the experiments; Hanlu Wang, Tiantian Yang, Yichao Yan, Fengmei Yang, Xunhuan Song, Shuning Zhang, Wenhong Jiang, Mingxue Li, Wenting Sun, Yanyan Li and Weihua Jin performed the experiments; Shuning Zhang specialized in the formal analysis of the work; Meng Qin provided constructive suggestions and opinions on immunologic animal experiment design; Fengmei Yang, Mingxue Li and Wenting Sun contributed

to authentic virus challenge; Hanlu Wang and Tiantian Yang also worked on the methodology; Yongping Jiang and Zhanlong He provided resources and supervised the validation work; Hanlu Wang and Tiantian Yang aided in data analysis; Hanlu Wang, Tiantian Yang and Suqin Duan wrote the manuscript; Yongping Jiang, Hanlu Wang and Tiantian Yang revised the manuscript. All the authors have read and approved the final manuscript.

Conflicts of interest

Dr. Yongping Jiang is the founder of Biopharmagen Corp. Hanlu Wang, Tiantian Yang, Yichao Yan, Shuning Zhang and Wenhong Jiang are employees of Biopharmagen Corp. All the remaining authors declare no competing interests. This does not alter our adherence to the journal policies on sharing data and materials.

Appendix A. Supporting information

Supporting information to this article can be found online at https://doi.org/10.1016/j.apsb.2025.11.027.

References

1. Chen B, Farzan M, Choe H. SARS-CoV-2 spike protein: structure, viral entry and variants. *Nat Rev Microbiol* 2025;**37**:455−68.
2. Al-Aly Z, Davis H, McCorkell L, Soares L, Wulf-Hanson S, Iwasaki A, et al. Long COVID science, research and policy. *Nat Med* 2024;**30**:2148−64.
3. Li JW, Zhou Y, Ma JC, Zhang Q, Shao J, Liang SF, et al. The long-term health outcomes, pathophysiological mechanisms and multidisciplinary management of long COVID. *Signal Transduct Targeted Ther* 2023;**8**:416.
4. Satterfield BA, Bhatt DL, Gersh BJ. Cardiac involvement in the long-term implications of COVID-19. *Nat Rev Cardiol* 2022;**19**:332−41.
5. Eligulashvili A, Darrell M, Gordon M, Jerome W, Fiori KP, Congdon S, et al. Patients with unmet social needs are at higher risks of developing severe long COVID-19 symptoms and neuropsychiatric sequela. *Sci Rep* 2024;**14**:7743.
6. Davis HE, McCorkell L, Vogel JM, Topol EJ. Long COVID: major findings, mechanisms and recommendations. *Nat Rev Microbiol* 2023; **21**:133−46.
7. Huang CL, Huang LX, Wang YM, Li X, Ren LL, Gu XY, et al. 6-month consequences of COVID-19 in patients discharged from hospital: a cohort study. *Lancet (London, England)* 2021;**397**:220−32.
8. Torres MKS, Bichara CDA, Almeida MNS, Vallinoto MC, Queiroz MAF, Vallinoto IMVC, et al. The complexity of SARS-CoV-2 infection and the COVID-19 pandemic. *Front Microbiol* 2022;**13**:789882.
9. Li GD, Hilgenfeld R, Whitley R, De Clercq E. Therapeutic strategies for COVID-19: progress and lessons learned. *Nat Rev Drug Discov* 2023;**22**:449−75.
10. Fang EY, Liu XH, Li M, Zhang ZL, Song LF, Zhu BY, et al. Advances in COVID-19 mRNA vaccine development. *Signal Transduct Targeted Ther* 2022;**7**:94.
11. Hu LD, Sun JM, Wang Y, Tan DY, Cao ZK, Gao LP, et al. A review of inactivated COVID-19 vaccine development in China: focusing on safety and efficacy in special populations. *Vaccines* 2023;**11**:1045.
12. Jacob-Dolan C, Barouch DH. COVID-19 vaccines: adenoviral vectors. *Annu Rev Med* 2022;**73**:41−54.
13. Pollet J, Chen WH, Strych U. Recombinant protein vaccines, a proven approach against coronavirus pandemics. *Adv Drug Deliv Rev* 2021; **170**:71−82.
14. Bravo L, Smolenov I, Han HH, Li P, Hosain R, Rockhold F, et al. Efficacy of the adjuvanted subunit protein COVID-19 vaccine, SCB-2019: a phase 2 and 3 multicentre, double-blind, randomised, placebo-controlled trial. *Lancet (London, England)* 2022;**399**:461−72.
15. Zhao X, Zhang R, Qiao ST, Wang X, Zhang WB, Ruan WJ, et al. Omicron SARS-CoV-2 neutralization from inactivated and ZF2001 vaccines. *N Engl J Med* 2022;**387**:277−80.
16. Hou YY, Chen M, Bian Y, Zheng X, Tong RS, Sun X. Advanced subunit vaccine delivery technologies: from vaccine cascade obstacles to design strategies. *Acta Pharm Sin B* 2023;**13**:3321−38.
17. Davies NG, Abbott S, Barnard RC, Jarvis CI, Kucharski AJ, Munday JD, et al. Estimated transmissibility and impact of SARS-CoV-2 lineage B.1.1.7 in England. *Science* 2021;**372**:eabg3055.
18. Tegally H, Wilkinson E, Giovanetti M, Iranzadeh A, Fonseca V, Giandhari J, et al. Detection of a SARS-CoV-2 variant of concern in South Africa. *Nature* 2021;**592**:438−43.
19. Faria NR, Mellan TA, Whittaker C, Claro IM, Candido DDS, Mishra S, et al. Genomics and epidemiology of the P.1 SARS-CoV-2 lineage in Manaus, Brazil. *Science* 2021;**372**:815−21.
20. Earnest R, Uddin R, Matluk N, Renzette N, Turbett SE, Siddle KJ, et al. Comparative transmissibility of SARS-CoV-2 variants delta and alpha in New England, USA. *Cell Rep Med* 2022;**3**:100583.
21. Davies NG, Jarvis CI, Edmunds WJ, Jewell NP, Diaz-Ordaz K, Keogh RH. Increased mortality in community-tested cases of SARS-CoV-2 lineage B.1.1.7. *Nature* 2021;**593**:270−4.
22. Funk T, Pharris A, Spiteri G, Bundle N, Melidou A, Carr M, et al. Characteristics of SARS-CoV-2 variants of concern B.1.1.7, B.1.351 or P.1: data from seven EU/EEA countries, weeks 38/2020 to 10/2021. *Euro Surveill* 2021;**26**:2100348.
23. Aleem A, Akbar Samad AB, Vaqar S. Emerging variants of SARS-CoV-2 and novel therapeutics against coronavirus (COVID-19). *StatPearls (Internet)* 2023. Available from: https://www.ncbi.nlm.nih.gov/books/NBK570580/.
24. Collier DA, DeMarco A, Ferreira I, Meng B, Datir RP, Walls AC, et al. Sensitivity of SARS-CoV-2 B.1.1.7 to mRNA vaccine-elicited antibodies. *Nature* 2021;**593**:136−41.
25. Jangra S, Ye CJ, Rathnasinghe R, Stadlbauer D, Krammer F, Simon V, et al. SARS-CoV-2 spike E484K mutation reduces antibody neutralisation. *Lancet Microbe* 2021;**2**:e283−4.
26. Cele S, Gazy I, Jackson L, Hwa SH, Tegally H, Lustig G, et al. Escape of SARS-CoV-2 501Y.V2 from neutralization by convalescent plasma. *Nature* 2021;**593**:142−6.
27. Zhou DM, Dejnirattisai W, Supasa P, Liu C, Mentzer AJ, Ginn HM, et al. Evidence of escape of SARS-CoV-2 variant B.1.351 from natural and vaccine-induced sera. *Cell* 2021;**184**:2348−61.e6.
28. Cao YL, Wang J, Jian FC, Xiao TH, Song WL, Yisimayi A, et al. Omicron escapes the majority of existing SARS-CoV-2 neutralizing antibodies. *Nature* 2022;**602**:657−63.
29. Senevirathne TH, Wekking D, Swain JWR, Solinas C, De Silva P. COVID-19: from emerging variants to vaccination. *Cytokine Growth Factor Rev* 2024;**76**:127−41.
30. Yi DR, Zhang YX, Wang J, Liu Q, Ma L, Li QJ, et al. Protection efficacy of mRNA-based SARS-CoV-2 variant vaccine in non-human primates. *Acta Pharm Sin B* 2025;**15**:934−46.
31. Rosenblum HG, Gee J, Liu RL, Marquez PL, Zhang BC, Strid P, et al. Safety of mRNA vaccines administered during the initial 6 months of the US COVID-19 vaccination programme: an observational study of reports to the vaccine adverse event reporting system and v-safe. *Lancet Infect Dis* 2022;**22**:802−12.
32. Wu S, Zhang LM, Wang WZ. Screened α-helix peptide inhibitor toward SARS-CoV-2 by blocking a prion-like domain in the receptor binding domain. *Anal Chem* 2022;**94**:11464−9.
33. Chen B. Molecular mechanism of HIV-1 entry. *Trends Microbiol* 2019;**27**:878−91.
34. Cantuti-Castelvetri L, Ojha R, Pedro LD, Djannatian M, Franz J, Kuivanen S, et al. Neuropilin-1 facilitates SARS-CoV-2 cell entry and infectivity. *Science* 2020;**370**:856−60.
35. Wang K, Chen W, Zhang Z, Deng YQ, Lian JQ, Du P, et al. CD147-spike protein is a novel route for SARS-CoV-2 infection to host cells. *Signal Transduct Targeted Ther* 2020;**5**:283.
36. Bermejo-Jambrina M, Eder J, Kaptein TM, Hamme JL, Helgers LC, Vlaming KE, et al. Infection and transmission of

SARS-CoV-2 depend on heparan sulfate proteoglycans. *EMBO J* 2021;**40**:e106765.
37. Lu Y, Shen F, He WQ, Li AQ, Li MH, Feng XL, et al. HR121 targeting HR2 domain in S2 subunit of spike protein can serve as a broad-spectrum SARS-CoV-2 inhibitor *via* intranasal administration. *Acta Pharm Sin B* 2023;**13**:3339−51.
38. Yan L, Wang FL, Hill M, Brun J, Liang Z, Shi XY, et al. A broadly neutralizing antibody recognizes a unique epitope with a signature motif common across coronaviruses. *Nat Commun* 2025;**16**:7580.
39. Qin SG, Huang H, Xiao W, Chen KP, He X, Tang XS, et al. A novel heterologous receptor-binding domain dodecamer universal mRNA vaccine against SARS-CoV-2 variants. *Acta Pharm Sin B* 2023;**13**:4291−304.
40. Wang Q, Sun LJ, Jiang SB. Potential recombination between SARS-CoV-2 and MERSCoV: calls for the development of Pan-CoV vaccines. *Signal Transduct Targeted Ther* 2023;**8**:122.
41. Li K, Li Z, Wohlford-Lenane C, Meyerholz DK, Channappanavar R, An D, et al. Single-dose, intranasal immunization with recombinant parainfluenza virus 5 expressing Middle East respiratory syndrome coronavirus (MERS-CoV) spike protein protects mice from fatal MERS-CoV infection. *mBio* 2020;**11**:e00554-20.
42. Tan ELC, Ooi EE, Lin CY, Tan HC, Ling AE, Lim B, et al. Inhibition of SARS coronavirus infection *in vitro* with clinically approved antiviral drugs. *Emerg Infect Dis* 2004;**10**:581−6.
43. Wang HL, Yang TT, Jiang WH, Qin M, Sun ZY, Dai W, et al. Identification and characterization of a novel cell binding and cross-reactive region on spike protein of SARS-CoV-2. *Sci Rep* 2022;**12**:15668.
44. Ren ZH, Wang YN, Jiang WH, Dai W, Jiang YP. Anti-tumor effect of a novel soluble recombinant human endostatin: administered as a single agent or in combination with chemotherapy agents in mouse tumor models. *PLoS One* 2014;**9**:e107823.
45. Guan X, Qin M, Zhang Y, Wang YN, Shen B, Ren ZH, et al. Safety and efficacy of megakaryocytes induced from hematopoietic stem cells in murine and nonhuman primate models. *Stem Cells Transl Med* 2017;**6**:897−909.
46. Zhang Y, Shen B, Guan X, Qin M, Ren ZH, Ma YP, et al. Safety and efficacy of *ex vivo* expanded $CD34^+$ stem cells in murine and primate models. *Stem Cell Res Ther* 2019;**10**:173.
47. Qin M, Guan X, Zhang Y, Shen B, Liu F, Zhang QY, et al. Evaluation of *ex vivo* produced endothelial progenitor cells for autologous transplantation in primates. *Stem Cell Res Ther* 2018;**9**:14.
48. Fan J, Ding XX, Jiang YP. A novel monoclonal antibody of human stem cell factor inhibits umbilical cord blood stem cell *ex vivo* expansion. *J Hematol Oncol* 2012;**5**:73.
49. Wang HL, Zhang YB, Yang HP, Qin M, Ding XX, Liu RH, et al. *In vivo* SELEX of an inhibitory NSCLC-specific RNA aptamer from PEGylated RNA library. *Mol Ther Nucleic Acids* 2018;**10**:187−98.
50. Wang HL, Qin M, Liu RH, Ding XX, Chen ISY, Jiang YP. Characterization of A bifunctional synthetic RNA aptamer and A truncated form for ability to inhibit growth of non-small cell lung cancer. *Sci Rep* 2019;**9**:18836.
51. Cerutti G, Guo YC, Liu LH, Liu LY, Zhang ZN, Luo Y, et al. Cryo-EM structure of the SARS-CoV-2 Omicron spike. *Cell Rep* 2022;**38**:110428.
52. Fraser BJ, Beldar S, Seitova A, Hutchinson A, Mannar D, Li YJ, et al. Structure and activity of human TMPRSS2 protease implicated in SARS-CoV-2 activation. *Nat Chem Biol* 2022;**18**:963−71.
53. Wrobel AG, Benton DJ, Xu PQ, Roustan C, Martin SR, Rosenthal PB, et al. SARS-CoV-2 and bat RaTG13 spike glycoprotein structures inform on virus evolution and furin-cleavage effects. *Nat Struct Mol Biol* 2020;**27**:763−7.
54. Kreutzberger AJB, Sanyal A, Saminathan A, Bloyet LM, Stumpf S, Liu Z, et al. SARS-CoV-2 requires acidic pH to infect cells. *Proc Natl Acad Sci U S A* 2022;**119**:e2209514119.
55. Rath SL, Kumar K. Investigation of the effect of temperature on the structure of SARS-CoV-2 spike protein by molecular dynamics simulations. *Front Mol Biosci* 2020;**7**:583523.
56. Zhang Q, Pavlinov I, Ye YH, Zheng W. Therapeutic development targeting host heparan sulfate proteoglycan in SARS-CoV-2 infection. *Front Med* 2024;**11**:1364657.
57. Olmedillas E, Rajamanickam RR, Avalos RD, Sosa FA, Zandonatti MA, Harkins SS, et al. Structure of a SARS-CoV-2 spike S2 subunit in a pre-fusion, open conformation. *Cell Rep* 2025;**44**:116052.
58. Park YJ, Walls AC, Wang ZQ, Sauer MM, Li WT, Tortorici MA, et al. Structures of MERS-CoV spike glycoprotein in complex with sialoside attachment receptors. *Nat Struct Mol Biol* 2019;**26**:1151−7.
59. Xia LY, Zhang YY, Zhou Q. Structural basis for the recognition of HCoV-HKU1 by human TMPRSS2. *Cell Res* 2024;**34**:526−9.
60. Hulswit RJG, Lang YF, Bakkers MJG, Li WT, Li ZS, Schouten A, et al. Human coronaviruses OC43 and HKU1 bind to 9-*O*-acetylated sialic acids *via* a conserved receptor-binding site in spike protein domain A. *Proc Natl Acad Sci U S A* 2019;**116**:2681−90.
61. Moura TR, Purta E, Bernat A, Martín-Cuevas EM, Kurkowska M, Baulin EF, et al. Conserved structures and dynamics in 5′-proximal regions of Betacoronavirus RNA genomes. *Nucleic Acids Res* 2024;**52**:3419−32.
62. Pereira Neto TA, Zmasek C, Avalos L, Sidney J, Trevizani R, Phillips E, et al. Highly conserved Betacoronavirus sequences are broadly recognized by human T cells. *Cell* 2025;**188**:5653−65.